

Ultrastructural Synaptic Changes Associated with Neurofibromatosis Type 1:
A Quantitative Analysis of Hippocampal Region CA1 in a Nf1^{+/-} Mouse Model

Armstrong, B.C.¹, LeBoutillier, J.C.² and, Petit, T.L.²

1. Department of Psychology and Center for the Neural Basis of Cognition

Carnegie Mellon University, Pittsburgh, PA, 15213

2. Department of Psychology

University of Toronto Scarborough, Toronto, ON M1C 1A4

Running Title: NF1 Ultrastructure

Key words: NF1, synaptic ultrastructure, CA1, hippocampus

ABSTRACT

Neurofibromatosis type 1 (NF1) is one of the most frequently diagnosed autosomal dominant inherited disorders resulting in neurological dysfunction, including an assortment of learning disabilities and cognitive deficits. To elucidate the neural mechanisms underlying the disorder, we employed a mouse model ($Nf1^{+/-}$) to conduct a quantitative analysis of ultrastructural changes associated with the NF1 disorder. Using both serial light and electron microscopy, we examined reconstructions of the CA1 region of the hippocampus, which is known to play a central role in many of the dysfunctions associated with NF1. In general, the morphology of synapses in both the $Nf1^{+/-}$ and wild-type groups of animals were similar. No differences were observed in synapse per neuron density, pre- and post- synaptic areas, or lengths. However, concave synapses were found to show a lower degree of curvature in the $Nf1^{+/-}$ mutant than in the wild type. These results indicate that the synaptic ultrastructure of $Nf1^{+/-}$ mice appears relatively normal with the exception of the degree of synaptic curvature in concave synapses, adding further support to the importance of synaptic curvature in synaptic plasticity, learning and memory.

INTRODUCTION

Neurofibromatosis type 1 (NF1) is an autosomal-dominant inherited disorder in which the normal functioning of the NF1 gene on chromosome 17 has been impaired (Viskochil, 2002). The NF1 gene normally serves to produce a cytoplasmic protein product, Neurofibromin, which acts as a tumor suppressor by reducing cell proliferation through the accelerated inactivation of a cellular proto-oncogene, p21 Ras (Basu et al., 1992; Costa et al., 2002). The NF1 disorder has been characterized at a neurobiological level by neurofibromas, benign tumors of the peripheral nervous system, and malignant peripheral nerve sheath tumors (Stephens et al., 1987). Behavioral testing has also linked NF1 with a variety of cognitive impairments including learning disabilities in 30-60% of afflicted children (North, 2000), low IQ (Greenwood et al., 2005; Levine et al., 2006), language difficulties (Billingsley et al., 2003; Watt et al., 2008), and abnormal executive functioning (Descheemaeker et al., 2005). Further abnormalities in gross and fine motor control (Hyman et al., 2006; Feldmann et al., 2003) and psychosocial problems (North et al., 2002; Barton and North, 2004; Noll et al., 2007) have been reported. These debilitating consequences of NF1, coupled with its high prevalence of approximately 1 in 3000 world-wide (Young et al., 2002; Arun & Gutmann, 2004), provide converging motivations for developing a better understanding of the specific abnormalities in the neural machinery that lead to these cognitive and sensorimotor impairments.

To investigate the neural underpinnings of NF1, we employed a $Nf1^{+/-}$ mouse model. **A genome-wide overview of the molecular pathogenic abnormalities in the $Nf1^{+/-}$ mouse hippocampus showed that various NF1 affected genes play a critical role in synaptic plasticity (Park et al., 2009).** The utilization of such a model does

entail an additional burden in establishing the similarities between the model and the human syndrome of primary interest. However, models which satisfy this requirement can offer unique insight into the neural basis of a disease and have made invaluable contributions to our knowledge of a number of syndromes. For example, mouse models have established relations between changes in the length of post synaptic density (PSD) at CA1 excitatory synapses in Rett syndrome mutants (Moretti et al., 2006), increased total number of synaptic contacts in APP/PS1E9 transgenic AD mutant (West et al., 2009), increased density of inhibitory synapses in dystrophin-deficient mdx mutants (Miranda et al., 2009) and deficits in asymmetric synapses and lower CA1 neuronal density in Ts65Dn Downsyndrome mutants (Kurt et al., 2004). These findings contribute to our greater understanding of the ultrastructural consequences of genetic mutations, and in turn may help identify specific parameters to target during the development of improved treatments and therapeutic strategies.

In the case of the Nf1^{+/-} mouse model that we studied, which carries a heterozygous null mutation of the NF gene, a body of convergent evidence has previously been reported that establishes the validity and relevance of the Nf1^{+/-} mouse to human NF1. Genotypic analyses have revealed that Neurofibrin shows a greater than 98% similarity between the human and mouse (Bernards et al., 1993). NF1 gene mutations in both humans and mice also exhibit similar phenotypes including impaired visuospatial learning and attention (Costa and Silva, 2002; Ullrich et al., 2010). Of particular relevance to the present study have been reports of NF1 mice exhibiting spatial learning deficits resulting from increased Ras activity and deficits in LTP in the hippocampus (Costa et al., 2001, 2002; Li et al., 2005). These observations, coupled with the wide

body of literature which has established that hippocampal LTP is associated with synaptically-mediated neural plasticity (Desmond and Levy 1983, 1988; Weeks et al., 1998, 1999, 2001; Geinisman et al., 1991, 1996) provide strong support that differences in synaptic ultrastructure and morphology in $Nf1^{+/-}$ mice might provide important insights into human NF1.

Past work also helps identify which aspects of synaptic ultrastructure and synaptic morphology are prime candidates for supporting neural plasticity relevant to the deficits documented in NF1. The first such candidate is changes in synaptic density, which are ubiquitous in studies of neural plasticity in development/aging (Crain et al, 1973, Bertoni-Feddari et al., 1986), enrichment (Van Reempts et al., 1992), synaptogenesis (Anthes et al., 1993) and LTP (Stewart et al., 2000). A second aspect of synaptic ultrastructure shown to be involved in neural plasticity are changes in the proportion of various synaptic subtypes (e.g., macular vs. perforated; Weeks et al., 1999; 2000) and the related measure of pre-synaptic curvature (Marrone et al., 2005), as differences in these measures may signal changes in the density/efficacy of synapses without modifying their total number. A third candidate mechanism is changes in pre-synaptic morphology. Morphologically docked vesicles at presynaptic active zones are thought to represent the anatomical correlate of the readily-releasable vesicle pool and show the same distribution across synapses (von Gersdorff et al., 1996; Schikorski & Stevens 1997; 2001; Murthy et al., 1997). More broadly, modulation of the number of docked vesicles has been linked to modulation of learning. For instance, increased numbers of docked vesicles have been observed in synapses from H-ras^{G12V} mice which show enhanced learning (Kushner et al., 2005), whereas decreased numbers of docked vesicles

have been reported in DKO mice with deletions in amyloid precursor protein and its homologue APP-like protein 2 (Yang et al, 2005). Reduced vesicle density has also been reported in the CA1 region of the UBE3A deficient mouse model for Angelman syndrome, another severe neurological disorder (Su et al., 2009).

Taken together, past research suggests that the deficits resulting from NF1 might be related to changes in synaptic ultrastructure and morphology on one of the three primary dimensions outlined above. An empirical examination of these dimensions would therefore make an important contribution to our understanding of the pathology of this disorder and, potentially, in the development of new treatments. To evaluate this hypothesis, in the current research we carried out a quantitative analysis of CA1 synapses reconstructed from serial microscopy for both wild-type (WT) controls and Nf1^{+/-} mutant mice.

MATERIALS AND METHODS

All live animal procedure, perfusions and initial tissue preparation were carried out in the Silva laboratory at University of California Los Angeles (UCLA) and all histological procedures were carried out in the Petit laboratory at the University of Toronto Scarborough (UTSC). To ensure that the research was conducted blind, the animals from both groups were coded at UCLA and the code was not released to the Petit laboratory until data were collected, entered, and ready for statistical analysis.

Animals

The experimental subjects were 12 **male** mice (6 WT controls and 6 Nf1^{+/-} mutants) approximately 5 months of age. Generation of the different genetically modified mice has been previously described (Jacks et al., 1994; Costa et al., 2002)

Perfusion Procedures

Mice were perfused following a modified version of the protocol described by Geinisman et al. (1993). The mice were deeply anesthetized and perfused transcardially with a prewash of phosphate buffered saline followed by 90 ml of universal fixative (1% paraformaldehyde, 1.25% glutaraldehyde, 0.2% CaCl in .12M phosphate buffer at pH 7.2) and finally 30 ml of a universal fixative with double the concentration of aldehydes solution. All solutions were heated to 37°C. Perfused animals were placed in sealed plastic bags and stored at 4°C for 2 hr. Brains were dissected from the animals and the whole brains immersed in the double concentration fixative overnight at 4°C, transferred to phosphate buffered solution for 24 hours, and shipped to UTSC. One of the WT brains was excluded from the study due to problems with fixation and embedding.

The hippocampus from the right side of the brain was extracted and processed for light and electron microscopy. Two 1 mm transverse hippocampal slices were removed from the mid-dorsal hippocampus with the aid of a dissecting scope. An area of CA1 midway between the CA2 and subicular regions and extending from CA1 through the dentate gyrus was removed. Each of these tissue blocks was divided in half, yielding four 0.5 mm sections and subsequently post-fixed for one hour at 4°C in 1 % osmium tetroxide (OsO₄) in .12M phosphate buffer at pH 7.2. Subsequently, the tissue was dehydrated in a graded series of ethanol solutions and embedded in Spurr's embedding medium (Ladd Research Industries, Burlington, VT). To ensure consistency between

groups in procedures that may affect tissue shrinkage and section thickness, all tissue was processed together for each step of histological processing.

Tissue Sectioning

Excess embedding medium was trimmed away from one randomly selected tissue block per animal. A series of 21 to 30 semi-thin (1 μ m thick) sections were cut for each animal using a Leica ultracut model UCT125 microtome and stained with Toluidine blue (1%). Completely trimmed semi-thin sections included the CA1 and dentate gyrus and were used for light microscopy neuronal quantification. These semi-thin sections were used to guide the subsequent trimming of each block to a trapezoidal area for serial EM sectioning. The targeted area was located in the middle third of stratum radiatum in CA1 between strata pyramidale and lacunosum moleculare. **The stratum radiatum was chosen since previous research has shown electrophysiological and/or synaptic ultrastructural changes in the stratum radiatum associated with altered learning in Nf1 mice (Cui et al., 2008), H-Ras mice (Kushner et al., 2005), and age-related spatial learning in rats (Nicholson et al., 2004).** Ultra-thin sections approximately 70 nm were subsequently taken from the tissue yielding a series of approximately 40 ultra-thin sections per block. Each series was mounted onto formvar slotted copper grids and counterstained with uranyl acetate and lead citrate.

Stereological methods

A stereological approach is required to correct for neuronal density changes due to any potential hypertrophy (Greenough et al., 1985) and to ensure that neurons are counted only once. The dissector method, a technique used to count objects without

making any assumptions regarding their size, shape or orientation, was used to obtain estimates of neuron density (Gundersen, 1977; Stereo, 1984; West 1999; 2002; Schmitz & Hof, 2005). In this study, in order to minimize or eliminate any potential tissue shrinkage differences, all measurements of neuronal and synaptic density were obtained from the same resin-embedded samples. Consequently, tissue shrinkage effects should have contributed equally to synaptic density and neuronal density data without biasing synapse number per neuron ratios.

Neuron Quantification

The entire CA1 cell body layer of the serial semi-thin sections was digitally photographed at 400x magnification on a Zeiss Axioplan 2 using Axiovision 4.2 software. Adobe Photoshop was used to view the images that had been captured. For those sections that had more than one image captured, a merging process was used to overlap the images onto a single template image. Neuronal nuclei were used as the counting unit and could be distinguished from those of glia by their morphological features and size. Neurons were counted by comparing adjacent thick sections, one serving as a reference section and the other as a look-up section. Neurons were counted only if they were observed in a reference section but not observed in the corresponding look—up section (Q-). The total volume for neuronal counting (V_{neur}) was derived as: $V_{neur} = A * H$ where A was the average area of the CA1 region determined with the Axiovision software and H was the total thickness of the series. **A total of 20 disector pairs were counted per animal, such that the total thickness was 20 μm for the series.** By dividing Q- by V_{neur} , a measure of neuron density, Nv_{neur} , was derived.

Synapse Quantification

Serial ultrathin sections were imaged using a Hitachi H-7500 transmission electron microscope and AnalySIS 3.0. The AnalySIS software package was used to digitally photograph the tissue, navigate through the digital images, and measure all morphological parameters. Photographs were aligned using tissue landmarks (e.g., a transversely sectioned myelinated fiber) as well as on-line viewing of previous micrographs, thus ensuring the same position was digitally captured on each section. A series of four digital electron micrographs of the targeted region were captured for each animal at a final magnification of 25,000X.

Synapses were identified by the presence of synaptic vesicles, dense material in a presynaptic axon terminal, and a corresponding PSD. Electron micrographs were zoomed electronically to provide enhanced accuracy during the stereological counting sequence. For each serial set of micrographs (reference and look-up) an unbiased sampling frame of 18.71 um^2 was predetermined and synapses were sampled. The number of synapses per counting frame (Q-) that were present in the reference section but disappeared in the look-up section was divided by the disector volume to derive the number of synapses in a given volume of tissue. The number of synapses per neuron was then determined by dividing the synaptic density, $N_{v_{\text{syn}}}$, by neuron density, $N_{v_{\text{neur}}}$.

Synaptic Structure

Synapses were classified using a similar system to Weeks et al., (1999; 2000; 2001). In addition to determining the total number of synapses per neuron, several other synaptic subtypes were examined (see Fig. 1). Initially, synapses were classified as either perforated (having a visible break in the PSD on any two-dimensional profile) or macular (non-perforated). Macular synapses were subsequently classified according to curvature

profile as follows: concave, a protrusion of the presynaptic terminal into the postsynaptic bouton; presynaptically convex, a protrusion of the postsynaptic bouton into the presynaptic terminal; flat, no discernable curvature; and irregular, more than one curvature configuration on consecutive sections (see Fig. 1). Synapses were also classified as either excitatory or inhibitory. Excitatory synapses, identified as having round vesicles and asymmetrical pre- and post-synaptic dense material, were distinguished from inhibitory synapses, identified as having oval vesicles and symmetrical dense material. The mean number of synapses per neuron was calculated for each of these subtypes for each animal. Unless otherwise noted, the data were analyzed using two-tailed independent sample t-tests, with an alpha of 0.05 and without assuming homogeneity of variance.

Reconstructed Synaptic Measures

Active Zone and Postsynaptic Density Areas

Complete profiles of the first 20 macular axospinous asymmetric synapses encountered per animal were reconstructed and analyzed as follows: First, the areas of the active zone and post-synaptic densities were measured in each individual section (see Fig. 2). The resulting product was then multiplied by the section thickness summed across the number of sections in which the synapse appeared. Measurements were performed with AnalySIS 3.0 software and Pearson product-moment correlations were determined to assess the relationship of these parameters.

Docked Vesicle Quantification

Docked vesicles were quantified for each of the reconstructed synapses. A vesicle was considered docked (see Fig. 3) when it was located immediately across from the PSD

and no visible separation occurred between vesicular and plasma membranes (Harris & Sultan, 1995; Schikorski & Stevens, 1997). Previous studies have shown that these vesicles accurately estimate those depleted during sustained repetitive activity. The total number of docked vesicles per synapse was counted and a measure of the area of the active zone per docked vesicle was calculated by dividing the total area by the number of vesicles docked for each synapse. Pearson product-moment correlations were calculated to assess the relationship between active zone size and the number of docked vesicles.

Synaptic Curvature and Length

Synaptic curvature was determined for all synapses with a clear PSD curvature on all profiles. For each synaptic length measured curvature was determined by taking the shape of the PSD as a uniform arc, determining this angle (θ_{PSD}), and deducing the angle of this arc from its origin θ^{ARC} using the following formula (Coxeter, 1963; see Marrone et al., 2005 for details).

$$\theta_{\text{ARC}} = 360 - (2\theta_{\text{PSD}})$$

Concave synapses were noted as positive angles and convex curvatures were noted as negative angles. The average degree of curvature and average and maximal synaptic length for each concave, convex and flat synaptic shape was calculated for each animal. For irregular and perforated synapses only length measurements were taken. For perforated synapses the length measurement did not include the perforation. These synaptic dimensions were analyzed using a two-tailed one-way analysis of variance with curvature as the single factor. Post hoc analysis were carried out using Fisher's least significant difference (LSD) procedure.

RESULTS

Neuronal Density

Serial semi-thin sections were examined at the light level for 11 animals (5 WT mice and 6 Nf1^{+/-}). The total number of neurons counted ranged from 43-178 per animal, with a mean of 98 ± 12.6 , through a mean volume of $41.4 \times 10^4 \pm 3.5 \times 10^4 \text{ um}^3$.

Neuronal density did not differ significantly between the Nf1^{+/-} ($29.68 \times 10^4 \pm 2.7479$ by $10^4/\text{mm}^3$) and WT ($29.72 \times 10^4 \pm 2.125 \times 10^4/\text{mm}^3$) groups, $t(9) = .01$.

Synaptic Density

A mean number of 228 ± 22 synapses was counted through a mean volume of $141 \pm 15.7 \text{ um}^3$ per animal. No difference in the mean total number of synapses per neuron in the Nf1^{+/-} (5762 ± 724) and WT (5597 ± 619) was observed, $t(9) = 0.16$. The proportions of synaptic types also did not differ. Table 1 summarizes the mean number of synapses per neuron for each synaptic type. Perforated synapses represented $8.1 \pm 0.7\%$ in the Nf1^{+/-} and $9.9 \pm 2.7\%$ in the WT groups. Inhibitory synapses represented $9.0 \pm 1.5\%$ of the total synapses in the Nf1^{+/-} group and $10.1 \pm 2.1\%$ of the total synapses in the WT group. Statistical tests revealed no significant differences on any density measures (all t-test p-values $> .09$).

Reconstructed Synaptic Measures:

Active Zone and Postsynaptic Density Areas

The active zone closely matched the PSD for all synapses measured (see Fig. 4A) for both Nf1^{+/-} ($r = 0.96$, $n = 120$) and WT ($r = 0.97$, $n = 100$). For both groups the active

zone areas were similar (Nf1^{+/-} = 0.0299 ± 0.001 um², range 0.008 - 0.067 um²; WT = 0.030 ± 0.001 um², range 0.009 - 0.069 um²).

Docked Vesicles

Although the active zone area and the number of docked vesicles varied from synapse to synapse, these 2 quantities were highly correlated (see Fig. 4B). No difference in the mean number of vesicles per active zone was observed (Nf1^{+/-} = 7.64 ± .31, WT = 8.26 ± 0.3). For the active zones sampled (Nf1^{+/-} n = 120; WT n = 100) the minimum number of docked vesicles was 2 and the maximum was 17 for both groups. The mean area per docked vesicle for each animal also did not differ between the groups (Nf1^{+/-} = 41 x 10⁻⁴um² ± 2 x 10⁻⁴; WT = 38 x 10⁻⁴ um² ± 1 x 10⁻⁴).

Synaptic Curvature and Length

Average synaptic curvature and length was determined by sampling 795 synapses (total WT = 394, Nf1^{+/-} = 401). Although there was a great deal of overlap between synapses of different curvature profiles, the average characteristics of these synapse populations was distinct. No significant differences were found on any synaptic length measures between conditions (all t-test p-values > .13; see Fig. 5).

The average degree of curvature of concave synapses was significantly lower in the Nf1^{+/-} (14.8° ± 1.2°) than the WT (18.0° ± 0.43°) groups, t(9) = .035. No significant differences were observed with convex synapses (WT = -18.7° ± 1.0°; Nf1^{+/-} = -19.8° ± 0.9°) and flat synapses (WT = 3.3° ± 0.5; Nf1^{+/-} = 2.5° ± 0.3°).

DISCUSSION

Cognitive impairment is present in approximately 50% of NF1 patients (Hyman, Shores & North, 2006) with NF1 mice exhibiting similar phenotypes. The current

research examined microscopy-based stereological characteristics of the synaptic phenotype in $Nf1^{+/-}$ mouse hippocampus to further our understanding of how these may contribute to the pathology of this disorder. Traditionally, researchers have focused on synaptic density and morphology to examine the underlying ultrastructural changes associated with learning and memory. While $Nf1^{+/-}$ mice perform more poorly on spatial tasks compared to WT, an in-depth examination of synaptic ultrastructure showed a generally normal histological organization, with the exception of a smaller degree of curvature in concave synapses.

Light microscopy results indicated there was no difference in the neuronal density between the two groups. The numbers obtained in this study (WT $29.72 \times 10^4/\text{mm}^3$) are similar to those reported by Kurt et al. (2004) in the CA1 region of control mice ($30.29 \times 10^4/\text{mm}^3$) but higher than those reported by Shi et al. (2005) in the young adult rat ($22.1872 \times 10^4/\text{mm}^3$). Interestingly, the current findings of no change in neuronal density in $Nf1^{+/-}$ mice are in contrast to those of Kurt and his colleagues' findings of decreased neuronal number in the Ts65Dn mouse which also showed impaired learning and memory on behavioral tasks. These researchers used mice 16-17 months of age and hence it is unclear whether it is the age difference, the difference between genetic mutations, or both parameters that underlie these divergent findings. The absence of change in neuronal density in the CA1 region of the mice examined in the current study suggests that other cellular and/or molecular differences may be critical factors underlying the observed behavioral deficits, and that the $Nf1^{+/-}$ mutation does not affect neurogenesis in this brain region.

Synaptic density measures examined in this study also did not differ between the WT and Nf1^{+/-} mutant. The number of inhibitory and excitatory synapses observed in the present work is similar to the number and distribution of inhibitory and excitatory synapses on rat hippocampal CA1 pyramidal cells reported by Megias et al. (2001). In the stratum radiatum of the rat, inhibitory synapses represent 18% of total synapses on thick medial dendrites and 3% on thin dendrites. Given our research did not discriminate between thick and thin dendrites, our results of approximately 10% symmetrical inhibitory synapses in the stratum radiatum for both the WT and Nf1^{+/-} group falls within this range. In contrast to the findings of Miranda et al. (2009), who reported a selective increase in inhibitory synapses without a change in global synaptic density in dystrophin-deficient mdx mice, our ultrastructural investigation does not suggest that there is a major reorganization of inhibitory circuits in Nf1^{+/-} mice at baseline. Recent research has shown that inhibitory synapses play an important role in Nf1^{+/-} mice, suggesting that future research may wish to focus on these synapses and their morphological plasticity in greater detail (Cui et al., 2008).

With respect to mean active zone and PSD areas, the Nf1^{+/-} mouse did not differ from WT. Similar to the findings of Schikorski and Stevens (1997), the active zone and PSD areas of each synapse were highly correlated in both groups of mice. This result suggests that these parameters also do not account for the deficits observed in these mice. The number of docked vesicles per active zone (Nf1^{+/-} = 7.64 ± 0.31 vs. WT = 8.26 ± 0.3) are smaller than values obtained by both Harris and Sultan (1995) who reported 15.6 vesicles (range = 2-36) per active zone, as well as Schikorski and Stevens (1997) who reported 10.3 vesicles per active zone (range = 2-27). In part, this may be

accounted for by the sampling procedures used by the different research labs. In the current study both multisynaptic and perforated synapses, which are among the largest synapses, were excluded. The present results of no differences between the WT and *Nf1*^{+/-} mutant on synaptic densities or docked vesicles are similar to the findings of Moretti et al. (2006) of no differences in docked vesicles or synaptic densities between the Rett syndrome *Mecp2*^{308/Y} mouse model and control mouse. However, whereas Moretti et al. reported decreases in PSD length in a Rett syndrome *Mecp2*^{308/Y} mouse model, the PSD lengths of the *Nf1*^{+/-} mouse did not differ from WT.

Synaptic shape may serve as a marker of processes involved with synaptic plasticity and is an intrinsic factor with its own functional implications (Markus & Petit, 1989, Medvedev et al. 2010). This may help explain the variations in synaptic curvature across synapses (Marrone et al., 2005). Several studies have reported that under conditions of plastic challenge, the proportions of different synaptic curvatures may change to include more concave and perforated synapses -- synaptic subtypes both thought to enhance efficacy (Weeks et al., 1999; 2000; 2001; Geinisman et al., 1993; see Marrone & Petit, 2002 for review). These inferences are supported by modeling work which has examined the effects of changing membrane geometry on synaptic function (Bertram et al., 1999, Ghaffari-Farazi et al., 1999). Simulations across realistic terminal morphologies have suggested that the more restricted the volume surrounding the release site, the higher the local concentration of calcium and the higher the probability of transmitter release with repetitive stimulation. For example, when a vesicle is docked near a point of concave inflection the probability of transmitter release increases, whereas the probability of transmitter release decreases for a vesicle docked near a point of

convex inflection (Ghaffari-Farazi et al.; Wu et al., 2003). It would be of interest in future research to examine synaptic structure in these animals following conditions of plastic challenge, such as LTP.

Together, the evidence from modelling and ultrastructural studies noted above indicates that changes in curvature are a morphological correlate of physiological activity, with fine-grained changes in curvature playing an important function in altered physiology and plasticity. The decreases in the degree of concavity in the Nf1 mutant as compared to the WT may contribute to altered synaptic efficacy at this synapse, contributing to the mutant animal's ability to learn less rapidly and efficiently than the wild type. The findings of the current study add to our further understanding of the importance of synaptic ultrastructure in general, and synaptic curvature in particular, in the processes of synaptic plasticity, learning and memory.

This research was supported by a grant from the Natural Sciences and Engineering Research Council to Ted L. Petit and an NSERC Post Graduate Scholarship to Blair C. Armstrong. The authors are thankful to Alcino Silva for supplying us with the animals used in this research, to Yijun Cui for her work in the perfusions and initial tissue preparation at UCLA, and to Gabriel Igorovan for assistance with data collection.

REFERENCES

- Anthes DL, LeBoutillier JC, Petit TL. 1993. Structure and plasticity of newly formed adult synapses: a morphometric study in the rat hippocampus. *Brain Res* 626(1-2):50-62.
- Arun D, Gutmann DH. 2004. Recent advances in neurofibromatosis type 1. *Curr Opin Neurol* 17(2):101-105.
- Barton B, North K. 2004. Social skills of children with neurofibromatosis type 1. *Dev Med Child Neurol* 46(8):553-563.
- Basu TN, Gutmann DH, Fletcher JA, Glover TW, Collins FS, Downward J. 1992. Aberrant regulation of ras proteins in malignant tumour cells from type 1 neurofibromatosis patients. *Nature* 356 (6371):713-715.
- Bernards A, Snijders AJ, Hannigan GE, Murthy AE, Gusella JF. 1993. Mouse neurofibromatosis type 1 cDNA sequence reveals high degree of conservation of both coding and non-coding mRNA segments. *Hum Mol Genet* 2(6):645-650.
- Bertram R, Smith GD, Sherman A. 1999. Modeling study of the effects of overlapping Ca^{2+} microdomains on neurotransmitter release. *Biophys. J.* 76:735-750.
- Bertoni-Freddari C, Giuli C, Pieri C, Paci D. 1986. Quantitative investigation of the morphological plasticity of synaptic junctions in rat dentate gyrus during aging. *Brain Res* 366(1-2):187-192.
- Billingsley RL, Slopis JM, Swank PR, Jackson EF, Moore III BD. 2003. Cortical morphology associated with language function in neurofibromatosis, type I. *Brain Lang* 85(1):125-139.
- Coxeter HSM. 1963. Introduction to geometry. HM Wiley & Sons. New York.
- Costa RM, Federov NB, Kogan JH, Murphy GG, Stern J, Ohno M, Kucherlapati R, Jacks T, Silva AJ. 2002. Mechanism for the learning deficits in a mouse model of neurofibromatosis type 1. *Nature* 415:526-530.
- Costa RM, Silva AJ. 2002. Molecular and cellular mechanisms underlying the cognitive deficits associated with neurofibromatosis 1. *J Child Neurol* 17(8):622-626.
- Costa RM, Yang T, Huynh DP, Pulst SM, Viskochil DH, Silva AJ, Brannan CI. 2001. Learning deficits, but normal development and tumor predisposition, in mice lacking exon 23a of Nf1. *Nat Genet* 27(4):399-411.
- Crain B, Cotman C, Taylor D, Lynch G. 1973. A quantitative electron microscopic study of synaptogenesis in the dentate gyrus of the rat. *Brain Res* 63:195-204.
- Cui Y, Costa RM, Murphy GG, Elgersma Y, Zhu Y, Mody I, Silva AJ. 2008. Neurofibromin regulation of ERK signaling modulates GABA release and learning. *Cell* 135(3):549-560.
- Descheemaeker MJ, Ghesquière P, Symons H, Fryns JP, Legius E. 2005. Behavioural, academic and neuropsychological profile of normally gifted Neurofibromatosis type 1 children. *J Intell Disabil Res* 49(1):33-46.
- Desmond NL, Levy WB. 1983. Synaptic correlates of associative potentiation/depression: an ultrastructural study in the hippocampus. *Brain Res* 265(1):21-30.
- Desmond NL, Levy WB. 1988. Synaptic interface surface area increases with long-term potentiation in the hippocampal dentate gyrus. *Brain Res* 453(1-2):308-314.

- Feldmann R, Denecke J, Grenzebach M, Schuierer G, Weglage J. 2003. Neurofibromatosis type 1 - Motor and cognitive function and T2-weighted MRI hyperintensities. *Neurology* 61(12):1725-1728.
- Geinisman Y, deToledo-Morrell L, Morrell F. 1991. Induction of long-term potentiation is associated with an increase in the number of axospinous synapses with segmented postsynaptic densities. *Brain Res* 566(1-2):77-88.
- Geinisman Y, deToledo-Morrell L, Morrell F, Heller R, Rossi M, Parshall R. 1993. Structural synaptic correlate of long-term potentiation: formation of axospinous synapses with multiple, completely partitioned transmission zones. *Hippocampus* 3(4):435-446.
- Geinisman Y, Detoledo-Morrell L, Morrell F, Persina IS, Beatty MA. 1996. Synapse restructuring associated with the maintenance phase of hippocampal long-term potentiation. *J Comp Neurol* 368(3):413-423.
- Ghaffari-Farazi T, Liaw J, Berger TW. 1999. Consequence of morphological alterations on synaptic function. *Neurocomput* 26:17-27.
- Greenwood RS, Tupler LA, Whitt JK, Butt A, Dombeck CB, Harp AG, Payne ME, Eastwood JD, Krishnan KRR, MacFall JR. 2005. Brain morphometry, T2-weighted hyperintensities, and IQ in children with neurofibromatosis type 1. *Arch Neurol-Chicago* 62(12):1904-1908.
- Harris KM, Sultan P. 1995. Variation in the number, location and size of synaptic vesicles provides an anatomical basis for the non-uniform probability of release at hippocampal CA1 synapses. *Neuropharm* 34(11):1387-1395.
- Hyman SL, Shores EA, North KN. 2006. Learning disabilities in children with neurofibromatosis type 1: subtypes, cognitive profile, and attention-deficit-hyperactivity disorder. *Dev Med Child Neurol* 48(12):973-977.
- Jacks T, Shih TS, Schmitt EM, Bronson RT, Bernards A, Weinberg RA. 1994. Tumour predisposition in mice heterozygous for a targeted mutation in *Nf1*. *Nature Gen* 7(3):353-361.
- Kurt AM, Kafa IM, Dierssen M, Davies CD. 2004. Deficits of neuronal density in CA1 and synaptic density in the dentate gyrus, CA3 and CA1, in a mouse model of Down syndrome. *Brain Res* 1022(1-2):101-109.
- Kushner SA, Elgersma Y, Murphy GG, Jaarsma D, van Woerden GM, Hojjati MR, Cui Y, LeBoutillier JC, Marrone DF, Choi ES, De Zeeuw CI, Petit TL, Pozzo-Miller L, Silva AJ. 2005. Modulation of presynaptic plasticity and learning by the H-ras/extracellular signal-regulated kinase/synapsin I signaling pathway. *J Neurosci* 25(42):9721-9734.
- Levine TM, Materek A, Abel J, O'Donnell M, Cutting LE. 2006. Cognitive profile of neurofibromatosis type 1. *Seminars in pediatric neurology* 13(1):8-20.
- Li W, Cui Y, Kushner SA, Brown RAM, Jentsch JD, Frankland PW, Cannon TD, Silva AJ. 2005. The HMG-CoA Reductase Inhibitor Lovastatin Reverses the Learning and Attention Deficits in a Mouse Model of Neurofibromatosis Type 1. *CurrBiol* 15(21):1961-1967.
- Markus EJ, Petit TL. 1989. Synaptic structural plasticity: Role of synaptic shape. *Synapse* 3:1-11.

- Markus EJ, Petit TL, LeBoutillier JC, Brooks WJ. 1994. Morphological characteristics of the synapse and their relationship to synaptic type: An electron microscopic examination of the neocortex and hippocampus of the rat. *Synapse* 17:65-68.
- Marrone DF, Petit TL. 2002. The role of synaptic morphology in neural plasticity: Structural interactions underlying synaptic power. *Brain Res Rev* 38 (3):291-308.
- Marrone DF, LeBoutillier JC, Petit TL. 2005. Ultrastructural correlates of vesicular docking in the rat dentate gyrus. *NeurosciLett* 378:92-97.
- Medvedev NI, Popov VI, Dallerac G, Davies HA, Laroche S, Kraev IV, Rodriguez Arellano JJ, Doyere V, Stewart MG. 2010. Synaptic curvature in the dentate gyrus following induction of long-term potentiation, long-term depression, and treatment with the N-methyl-d-aspartate receptor antagonist CPP. *Neurosci* 171:390-397.
- Megias M, Emri Z, Freund TF, Gulyas, AI. 2001. Total number and distribution of inhibitory and excitatory synapses on hippocampal CA1 pyramidal cells. *Neuroscience* 102:527-540.
- Miranda R, Sebric C, Degrouard J, Gillet B, Jaillard D, Laroche S, Vaillend C. 2009. Reorganization of inhibitory synapses and increased PSD length of perforated excitatory synapses in hippocampal area CA1 of dystrophin-deficient mdx mice. *Cerebral Cortex* 19:876-888.
- Moretti P, Levenson JM, Battaglia F, Atkinson R, Teague R, Antalffy B, Armstrong D, Arancio O, Sweatt J, Zoghbi HY. 2006. Learning and memory and synaptic plasticity are impaired in a mouse model of Rett Syndrome. *J Neurosci* 26(1):319-327.
- Murthy VN, Sejnowski TJ, Stevens CF. 1997. Heterogeneous release properties of visualized individual hippocampal synapses. *Neuron* 18(4):599-612.
- Nicholson DA, Yoshida R, Berry RW, Gallagher M, Geinisman Y. 2004. Reduction in size of perforated postsynaptic densities in hippocampal axospinous synapses and age-related spatial learning impairments. *J Neurosci* 24(35):7748-7653.
- Noll RB, Reiter-Purtill J, Moore BD, Schorry EK, Lovell AM, Vannatta K, Gerhardt CA. 2007. Social, emotional, and behavioral functioning of children with NF1. *Am J Med Genet* 143A(19):2261-2273.
- North K. 2000. Neurofibromatosis type 1. *Am J Med Genet* 97(2):119-127.
- North K, Hyman S, Barton B. 2002. Cognitive deficits in neurofibromatosis 1. *J Child Neurol* 17(8):605-612.
- Park CS, Zhong L, Tang S-J. 2009. Aberrant expression of synaptic plasticity-related genes in the Nf1^{+/-} mouse hippocampus. *J Neurosci Res* 87: 3107-3119.
- Schikorski T, Stevens CF. 1997. Quantitative ultrastructural analysis of hippocampal excitatory synapses. *J Neurosci* 17(15):5858-5867.
- Schikorski T, Stevens CF. 2001. Morphological correlates of functionally defined synaptic vesicle populations. *Nat Neurosci* 4(4): 391-395.
- Schmitz C, Hof PR. 2005. Design-based stereology in neuroscience. *Neuroscience* 130(4):813-831.
- Shi L, Linville MC, Tucker EW, Sonntag WE, Brunso-Bechtold JK. 2005. Differential Effects of Aging and Insulin-like Growth Factor-1 on Synapses in CA1 of Rat Hippocampus. *Cereb Cortex* 15(5):571-577.

- Stephens K, Riccardi VM, Rising M, Ng S, Green P, Collins FS, Rediker KS, Powers JA, Parker C, Donis-Keller H. 1987. Linkage studies with chromosome 17 DNA markers in 45 neurofibromatosis 1 families. *Genomics* 1(4): 353-357.
- Sterio D. 1984. The unbiased estimation of number and sizes of arbitrary particles using the disector. *J Microsc* 134:127-136.
- Stewart MG, Harrison E, Rusakov DA, Richter-Levin G, Maroun M. 2000. Re-structuring of synapses 24 hours after induction of long-term potentiation in the dentate gyrus of the rat hippocampus in vivo. *Neuroscience* 100(2):221-227.
- Su H, Fan W, Coskun PE, Vesa J, Gold J-A, Jiang Y-H, Potluri P, Procaccio V, Acab A, Weiss JH, Wallace DC, Kimonis VE. 2011. Mitochondrial dysfunction in CA1 hippocampal neurons of the UBE3A deficient mouse model for Angelman syndrome. *NeurosciLett* 487(2):129-133.
- Ulrich NJ, Ayr L, Leaffer E, Irons MB, Rey-Casserly G. 2010. Pilot study of a novel computerized task to assess spatial learning in children and adolescents. *J Child Neurol*. <http://jcn.sagepub.com/content/early/2010/02/05/0883073809358454>.
- Van-Reempts J, Dikova M, Werbrouck L, Clincke G, Borgers M. 1992. Synaptic plasticity in rat hippocampus associated with learning. *Behav Brain Res* 51(2):179-183.
- Von-Gersdorff H, Vardi E, Matthews G, Sterling P. 1996. Evidence that vesicles on the synaptic ribbon of retinal bipolar neurons can be rapidly released. *Neuron* 16(6):1221-1227.
- Viskochil D. 2002. Genetics of neurofibromatosis 1 and the NF1 gene. *J Child Neurol* 17(8):562-570.
- Watt SE, Shores A, North KN. 2008. An examination of lexical and sublexical reading skills in children with neurofibromatosis type 1. *Child Neuropsychol* 14(5):401-418.
- Weeks ACW, Ivanco TL, LeBoutillier JC, Racine RJ, Petit TL. 1998. The degree of potentiation is associated with synaptic number during the maintenance of long-term potentiation in the rat dentate gyrus. *Brain Res* 798(1-2):211-216.
- Weeks ACW, Ivanco TL, LeBoutillier JC, Racine RJ, Petit TL. 1999. Sequential Changes in the Synaptic Structural Profile Following Long-Term Potentiation in the Rat Dentate Gyrus: I. The Intermediate Maintenance Phase. *Synapse* 31(2):97-107.
- Weeks ACW, Ivanco TL, LeBoutillier JC, Racine RJ, Petit TL. 2000. Sequential changes in the synaptic structural profile following long-term potentiation in the rat dentate gyrus: II. Induction/early maintenance phase. *Synapse* 36:286-296.
- Weeks ACW, Ivanco TL, LeBoutillier JC, Racine RJ, Petit TL. 2001. Sequential changes in the synaptic structural profile following long-term potentiation in the rat dentate gyrus: III. Long-term maintenance phase. *Synapse* 40(1):74-84.
- West MJ. 1999. Stereological methods for estimating the total number of neurons and synapses: issues of precision and bias. *Trends Neurosci* 22(2):51-61.
- West MJ. 2002. Design-based stereological methods for counting neurons. *Prog Brain Res* 135: 43-51.
- West MF, Bacha G, Soderman A, Jensen JL. 2009. Synaptic contact number and size in stratum radiatum CA1 of APP/PS1_E9 transgenic mice. *Neurobiology of Aging* 30:1756-1776.

- Wu GY, Kleim J, Marrone DF, Berger TW, Petit TL 2003. Morphological basis of neural plasticity. *CNS Drug Rev* 9:217.
- Yang G, Gong Y-D, Gong K, Jiang W-L, Kwon E, Wang P, Zheng H, Zhang X-F, Gan W-B, Zhao N-M. 2005. Reduced synaptic vesicle density and active zone size in mice lacking amyloid precursor protein (APP) and APP-like protein 2. *NeurosciLett* 384(1-2):66-71.
- Young H, Hyman S, North K. 2002. Neurofibromatosis 1: Clinical review and exceptions to the rules. *J Child Neurol* 17(8): 613-621.

Table Caption

Table 1 lists synapse per neuron ratios for various synaptic subtypes for Nf1^{+/-} and WT groups ¹ Values are provided as means \pm S.E.M

Synapse Type	Synapse per neuron			
	WT n=5		Nf1 ^{+/-} n=6	
	Mean	SEM ¹	Mean	SEM
Concave Macular	884	165	875	174
Convex Macular	2867	668	2933	642
Irregular Macular	239	70	290	87
Flat Macular	1110	157	1213	318
Total Macular Synapses	5100	660	5311	692
Total Perforated	497	64	450	47

¹SEM = standard error of the mean

Figure Captions

Fig. 1. Electromicrographs depicting: A) a concave synapse, B) a flat synapse, C) a convex synapse, and D) a perforated synapse. “Pre” and “Post” indicate the presynaptic and postsynaptic elements in each micrograph. The magnification bar in Fig. 1D indicates the magnification for all micrographs.

Fig. 2. Serial sections through a synapse. A. The first section to graze the synaptic contact; no active zone is showing in this section. B through D. Sections through the active zone. The curved arrows in Fig 2B indicate the length of the pre-synaptic active zone, while the straight arrows indicate the length of the post-synaptic density. E. The last section to graze the synaptic contact; no active zone is showing in this section. The magnification bar in Fig. 2E indicates the magnification for all images.

Fig. 3. Electromicrograph depicting a docked vesicle indicated by an arrowhead.

Fig. 4. Scatterplots of: A) Synaptic active zone area and PSD area for Nf1^{+/-} (n = 120, r = 0.96) and WT (n = 100, r = 0.97) and B) active zone area and corresponding number of docked vesicles for the synapses in 4A (correlation coefficient for NF1 = 0.9 and WT = 0.88).

Fig. 5 Measures of PSD length for different synaptic subtypes; no significant differences were observed between WT and Nf1^{+/-} synaptic subtypes.

Figure 1.

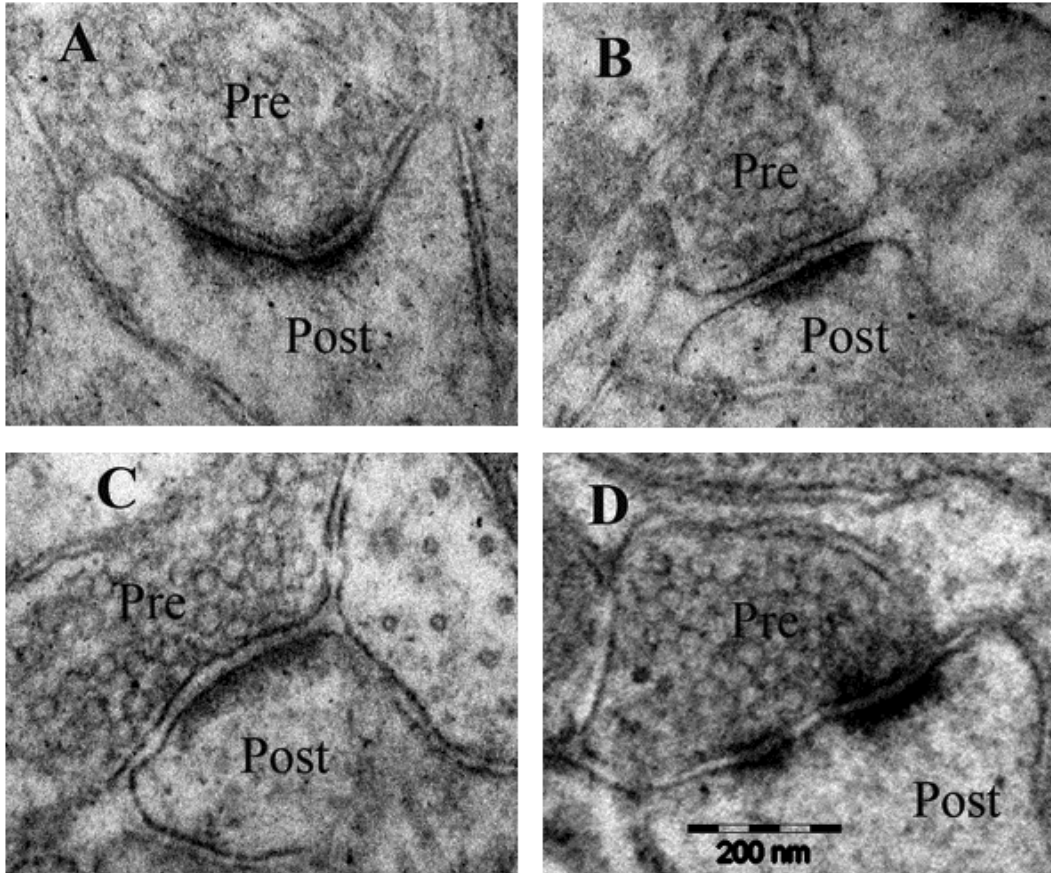


Figure 2.

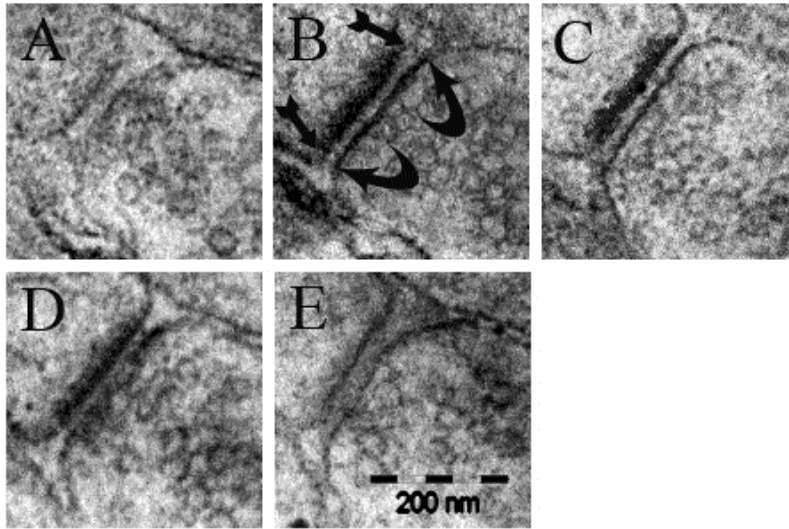


Figure 3.

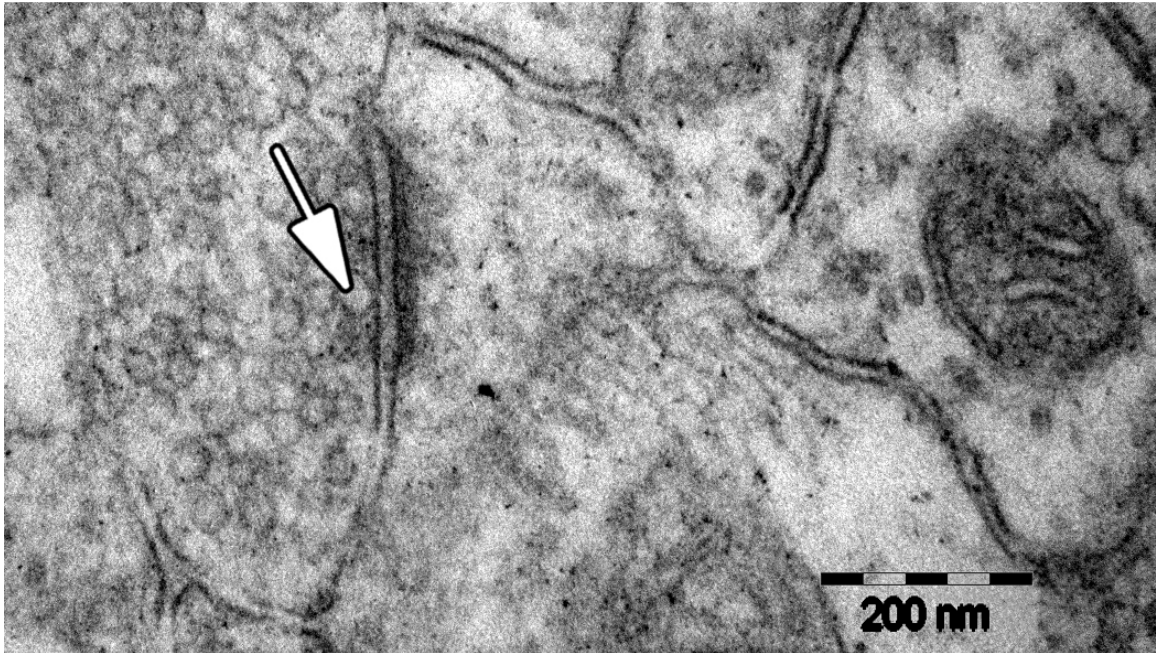


Figure 4A.

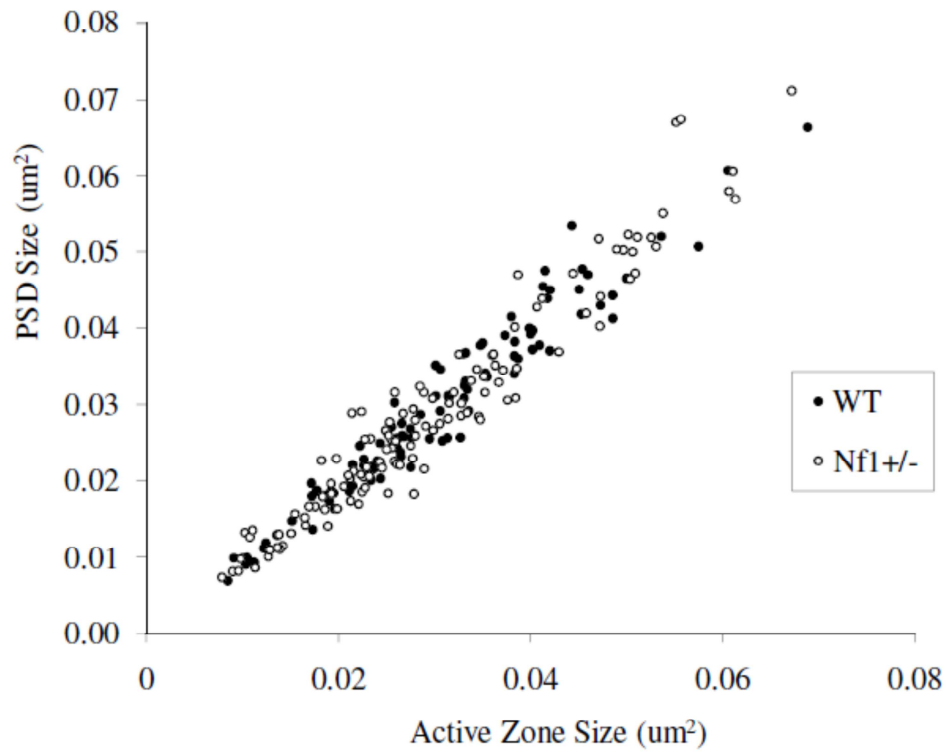


Figure 4B.

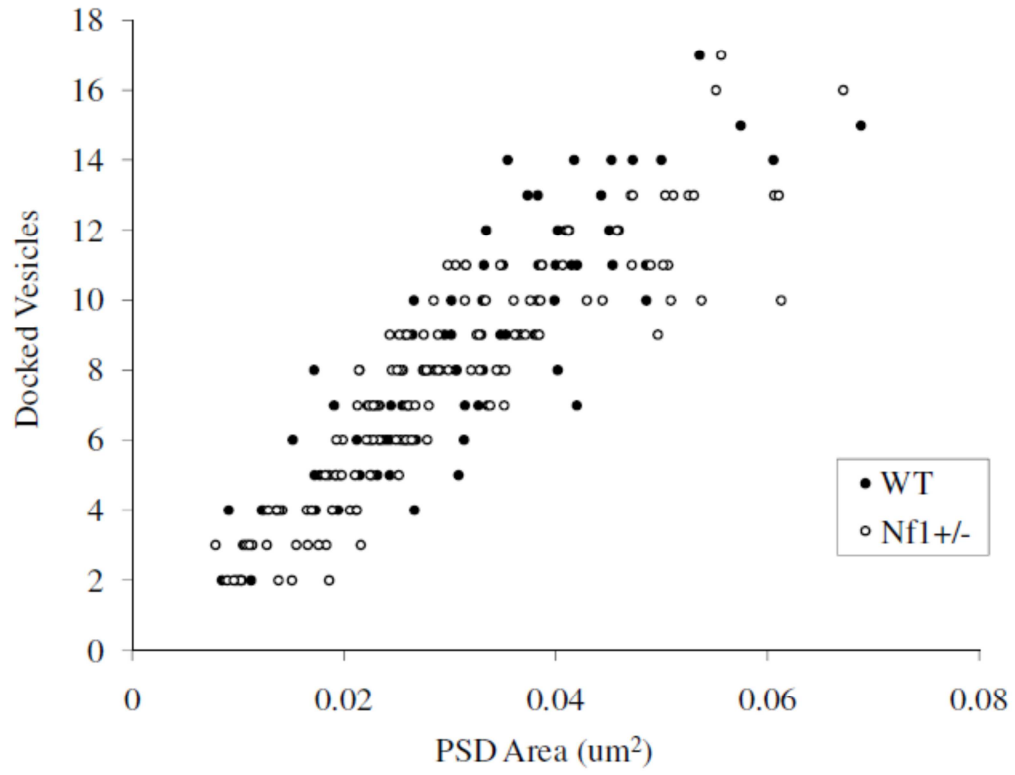


Figure 5.

